JOURNAL OF COMPUTATIONAL PHYSICS 33, 340–358 (1979)

On the Convergence of Numerical Solutions for 2-D Flows in a Cavity at Large Re

A. S. BENJAMIN* AND V. E. DENNY†

University of California, Energy and Kinetics Department, Los Angeles, California 90024

Received January 11, 1977

Convergence properties of various finite-difference schemes for solving the equations of motion for recirculating flow of an incompressible fluid in a square 2-D cavity are examined at Reynolds numbers up to 10^4. Stream function-vorticity forms of the governing equations are approximated by means of second-order-correct central-difference approximations and solved by means of alternating-direction-implicit iteration. The effects of grid-altering coordinate transformations, spatially nonuniform ADI relaxation parameters, and order-correct treatments of the vorticity boundary condition on such issues as accuracy and rate of convergence are established. Differences in results occurring with upwind versus central differencing at high Reynolds numbers are explained with consideration in particular for the sizes of the secondary vortices. Formulation of the advective terms in convective, divergence, and Arakawa-conservative forms is discussed in terms of global conservation of vorticity, kinetic energy, and square vorticity.

INTRODUCTION

The development of improved methods for solving the Navier–Stokes equations governing recirculating flows within closed streamlines has been a subject of concern to computational physicists for nearly two decades. Of particular concern are the difficulties associated with the nonlinear advective terms as the Reynolds number becomes large, which have frustrated efforts to obtain computationally stable and numerically accurate solutions at reasonable cost.

The magnitude of the difficulty is suggested by the fact that fully converged second-order-correct finite-difference solutions for the simple model problem of shear-driven flow in a square 2-D cavity have yet to be obtained at other than modest Reynolds numbers [1–5]. Although stable "solutions" have been generated at much larger Reynolds numbers [3, 6–8] using upwind differencing of the advective terms [9], it has been shown [4, 10] and will be shown later in this paper that the results are likely invalid owing to first-order false diffusion effects. These effects can to some extent be alleviated by employing higher-order-correct upwind differencing [11]; however, this approach introduces added complexity in relaxing the nonlinear algebraic problem by means of, for example, alternating-direction-implicit (ADI) methods [12].

* Current address: Sandia Laboratories, Albuquerque, N.M. 87185.
† Current address: Science Applications, Inc., Palo Alto, Calif. 94304.

0021-9991/79/120340–19$02.00/0

As might be expected, other computational approaches for solving the basic problem are being explored. For example, Chorin [13] introduced a method for solving the Navier–Stokes equations at high Reynolds numbers wherein vortex "blobs" are assigned over the flow field and then permitted to disperse according to a combination of deterministic guidelines and computer-generated pseudorandom numbers (random walks). Although application to transverse flow across an infinitely long cylinder is in good agreement with experiment for $500 \leqslant \mathrm{Re} \leqslant 5000$, the method is not applicable at low Reynolds numbers and has proven troublesome at very high Reynolds numbers owing to noise induced by oscillating vortices in boundary layer regions. The method has, however, been applied to the model 2-D cavity problem with some success [14].

In opposition to finite-difference methods of analysis are the methods of variational calculus wherein dependent variables are expanded in truncated sequences of spatially dependent functionals (trial functions), the coefficients in the resulting series approximations being extracted from simple integrations over the domain of interest followed by matrix inversion. An application [15] of this approach (often referred to as the Galerkin method) to the solution of thermally driven flow of a high Prandtl number Boussinesq fluid in a square 2-D cavity using beam functions was encouraging; however, the method tended to misrepresent more seriously the hydrodynamics of the problem than was the case for finite-difference solutions.

The purpose of the present contribution is to report recent progress on the application of finite-difference methods to the solution of the Navier–Stokes equations at large Reynolds numbers. The physical situation is one of steady recirculating flow of a viscous fluid in a square 2-D cavity, motion being induced by transverse movement of the top plate. Stream function-vorticity forms of the governing laminar equations are solved by means of second-order-correct central-difference approximations applied in a transformed coordinate system. The resulting nonlinear algebraic problem is relaxed by means of ADI methods using a nonuniform iteration parameter. Fully converged solutions at Reynolds numbers up to 10^4 are generated in order to resolve basic questions on the nature of the flow and to explore convergence properties of the method. The question of whether the flow is laminar or turbulent at such high Reynolds numbers is addressed under Results and Discussion.

Analysis

Governing Equations

For shear-driven flow of a viscous fluid in a square cavity, the governing equations may be written as

$$\frac{\partial \psi}{\partial t} = \omega + \nabla^2 \psi, \tag{1}$$

$$\frac{\partial \omega}{\partial t} = -\frac{\partial}{\partial x}\left(\frac{\partial \psi}{\partial y}\,\omega\right) + \frac{\partial}{\partial y}\left(\frac{\partial \psi}{\partial x}\,\omega\right) + \mathrm{Re}^{-1}\,\nabla^2 \omega, \tag{2}$$

where $\partial\psi/\partial y = u$, $-\partial\psi/\partial x = v$, $\mathrm{Re} = LU/\nu$, and false-transient terms are introduced as in Ref. [16]. For convenience in effecting more nearly optimal distributions of node points for the numerical solution, it being recognized that a greater density of nodes is desirable in the highly viscous boundary layer and secondary vortex (corner) regions than in the inviscid core, the governing equations are alternatively written in terms of coordinates

$$\xi = 0.5\{1 + \tan[(2x - 1)\beta]/\tan\beta\} \tag{3}$$

and

$$\eta = 0.5\{1 + \tan[(2y - 1)\beta]/\tan\beta\}. \tag{4}$$

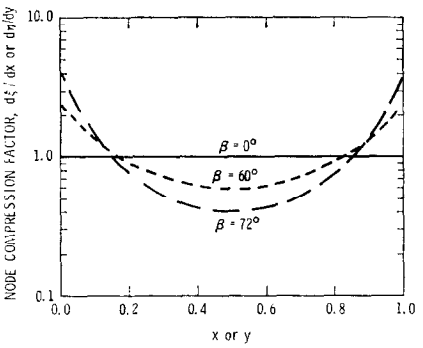

FIG. 1. Effect of coordinate transformation on node density distribution.

The nodal compression factor $d\xi/dx$ (or $d\eta/dy$) is illustrated in Fig. 1, where it may be observed (by comparison with Fig. 5, shown later) that the gradients introduced by the transformation are mild compared to the gradients of vorticity encountered in the physical problem. With the transformation, Eqs. (1) and (2) become

$$\frac{\partial\psi}{\partial t'} = \frac{\omega}{\xi_x\eta_y} + \frac{\partial}{\partial\xi}\left(\frac{\xi_x}{\eta_y}\frac{\partial\psi}{\partial\xi}\right) + \frac{\partial}{\partial\eta}\left(\frac{\eta_y}{\xi_x}\frac{\partial\psi}{\partial\eta}\right), \tag{5}$$

$$\frac{\partial\omega}{\partial t'} = -\frac{\partial}{\partial\xi}\left(\frac{\partial\psi}{\partial\eta}\omega\right) + \frac{\partial}{\partial\eta}\left(\frac{\partial\psi}{\partial\xi}\omega\right) + \mathrm{Re}^{-1}\left[\frac{\partial}{\partial\xi}\left(\frac{\xi_x}{\eta_y}\frac{\partial\omega}{\partial\xi}\right) + \frac{\partial}{\partial\eta}\left(\frac{\eta_y}{\xi_x}\frac{\partial\omega}{\partial\eta}\right)\right] \tag{6}$$

where it is to be noted that the product $\xi_x\eta_y$ of the metrics of the transformation has been absorbed in the false-transient terms.

Boundary conditions for the problem are

$$u = v = \psi = 0 \tag{7}$$

at

$$x = 0,\ y = 0,\ x = 1;$$

and

$$u = 1,\ v = \psi = 0 \tag{8}$$

at

$$y = 1.$$

Method of Solution

The governing equations were solved via the method of false transients [16], approximating spatial derivatives in ψ and ω in terms of three point central-difference analogs and relaxing the resulting nonlinear algebraic problem by means of ADI iteration. For (x, y) coordinates, the numerical algorithm takes the form

$$\begin{aligned} h^{-2}\sigma_\psi(\psi_{k+1/2} - \psi_k) - D_{xx}\psi_{k+1/2} - D_{yy}\psi_k - \omega_k &= O(h^2), \\ h^{-2}\sigma_\psi(\psi_{k+1} - \psi_{k+1/2}) - D_{xx}\psi_{k+1/2} - D_{yy}\psi_{k+1} - \omega_k &= O(h^2) \end{aligned} \tag{9}$$

and

$$\begin{aligned} &h^{-2}\sigma_\omega(\omega_{k+1/2} - \omega_k) + D_x(u_{k+1}\omega_{k+1/2}) + D_y(v_{k+1}\omega_k) \\ &\quad - \mathrm{Re}^{-1} D_{xx}\omega_{k+1/2} - \mathrm{Re}^{-1} D_{yy}\omega_k = O(h^2), \\ &h^{-2}\sigma_\omega(\omega_{k+1} - \omega_{k+1/2}) + D_x(u_{k+1}\omega_{k+1/2}) + D_y(v_{k+1}\omega_{k+1}) \\ &\quad - \mathrm{Re}^{-1} D_{xx}\omega_{k+1/2} - \mathrm{Re}^{-1} D_{yy}\omega_{k+1} = O(h^2), \end{aligned} \tag{10}$$

where

$$\begin{aligned} D_x\phi &= [\phi(x + h, y) - \phi(x - h, y)]/2h, \\ D_{xx}\phi &= [\phi(x + h, y) - 2\phi(x, y) + \phi(x - h, y)]/h^2, \\ &\text{etc.}, \end{aligned}$$

and

$$\sigma_\psi = h^2/\Delta t_\psi\,, \qquad \sigma_\omega = h^2/\Delta t_\omega\,.$$

(The notation Δt_ψ and Δt_ω has been introduced to indicate that the false-transient terms do not require that the pseudotime steps of the stream function/vorticity equations be equal.) As usual, the indices $k \to k + \frac{1}{2} \to k + 1$ denote one cycle of the ADI iterative process.

Numerical evaluation of the vorticity at the walls intermediate between application of Eqs. (9) and (10) was effected in terms of the following alternatives:

$$(\omega_B)_{k+1} = -\frac{2\psi_{B-1}}{h^2} - \frac{2}{h}\left(\frac{\partial\psi}{\partial n}\right)_B + O(h), \tag{11}$$

$$(\omega_B)_{k+1} = -\frac{8\psi_{B-1} - \psi_{B-2}}{2h^2} - \frac{3}{h}\left(\frac{\partial\psi}{\partial n}\right)_B + O(h^2), \tag{12}$$

$$(\omega_B)_{k+1} = -\frac{21\psi_{B-1} - 6\psi_{B-2} + \psi_{B-3}}{3h^2} - \frac{4}{h}\left(\frac{\partial\psi}{\partial n}\right)_B + O(h^3), \tag{13}$$

where B, $B-1$, etc., denote node points on the wall, one point in from the wall, etc.; n is measured perpendicular to the wall and outward from the center of the cavity; and $(\partial\psi/\partial n)_B = 1$ at $y = 1$ and vanishes at the other surfaces. As discussed in Ref. [15], near-optimal relaxation of the nonlinear problem is obtained by damping ω_B via

$$(\omega_B)_{k+1} = (1 - \sigma_B)_k(\omega_B)_k + \sigma_B(\omega_B)_{k+1} \tag{14}$$

with $\sigma_B = 0.15$.

The numerical algorithm for the problem in (ξ, η) coordinates is similar in form; details are given in Ref. [17]. In either formulation, the overall method of solution involves the following sequential steps:

(i) construct initial distributions of ψ and ω;

(ii) advance ψ-equation 1 cycle;

(iii) advance ω_B,

(iv) advance ω-equation 1 cycle;

(v) determine root-mean-square residuals (see Results and Discussion)

(vi) repeat steps (ii)–(v) until convergence is obtained.

(Actually, solutions were generated at sequences of Reynolds numbers, using converged solutions at a previous Reynolds number as the initial condition for a subsequent Reynolds number.)

Nonuniform σ_ω

Numerical experiments with a constant σ_ω applied uniformly over the domain revealed that high values of the parameter were required in order to stabilize the solution in regions of high vorticity gradients, but that these high values of σ_ω were overly restrictive in the central core region where changes tended to occur very slowly. To speed the overall convergence of the numerical equations, a nonuniform iteration parameter was postulated based on a von Neumann stability analysis whose details

are given in [17]. (Although the von Neumann method is not globally applicable for problems with variable coefficients and mixed boundary conditions, it has been shown [18, 19] that satisfactory results can be obtained on a local basis even when these conditions exist.) The essential features of the derivation are as follows.

Substituting

$$\psi_k = \psi_\infty + \delta\psi_k = \psi_\infty + A_{p,q,k} \exp[2\pi i(px + qy)/h]$$

and

$$\omega_k = \omega_\infty + \delta\omega_k = \omega_\infty + B_{p,q,k} \exp[2\pi i(px + qy)/h]$$

into both parts of Eqs. (9) and (10), but using the convective form of the latter to simplify the algebra, there result four equations which enable $A_{p,q,k+1}$ and $B_{p,q,k+1}$ to be calculated given $A_{p,q,k}$ and $B_{p,q,k}$. Considerable algebraic complication can be avoided by assuming that terms of order $\delta\psi \cdot \delta\omega$ are negligible and that $\omega_k + \nabla^2\psi_k = 0$ (i.e., that the residual of Eq. (9) is much smaller than that of Eq. (10) in the regions of primary interest), after which a single (complex) equation for the amplification ratio, $B_{p,q,k+1}/B_{p,q,k}$, can be derived. Examining two limits of the equation, it develops that

$$\left|\frac{B_{p,q,k+1}}{B_{p,q,k}}\right|^2 = \frac{[\sigma_\omega - 4\sin^2(\pi p)]^2 + [\mathrm{Re}\, hu_{i,j}\sin(2\pi p)]^2}{[\sigma_\omega + 4\sin^2(\pi p)]^2 + [\mathrm{Re}\, hu_{i,j}\sin(2\pi p)]^2} \times \frac{[\sigma_\omega - 4\sin^2(\pi q)]^2 + [\mathrm{Re}\, hv_{i,j}\sin(2\pi q)]^2}{[\sigma_\omega + 4\sin^2(\pi q)]^2 + [\mathrm{Re}\, hv_{i,j}\sin(2\pi q)]^2} \tag{15}$$

when the vorticity gradients are very small, attesting to the stability of the method in the invariant core (since the amplification ratio is less than unity); whereas

$$\left|\frac{B_{p,q,k+1}}{B_{p,q,k}}\right|^2 = 1 + \left\{\frac{\mathrm{Re}\, h^2[(\omega_{i+1,j} - \omega_{i-1,j})\sin(2\pi p) - (\omega_{i,j+1} - \omega_{i,j-1})\sin(2\pi q)]}{4\sigma_\omega[\sin^2(\pi p) + \sin^2(\pi q)]}\right\}^2 \tag{16}$$

when the vorticity gradients are very large (and σ_ω is also very large), illustrating the basic instability of such regions of the flow. In practice, it is possible to maintain stability by decreasing h and increasing σ_ω, both of which tend to reduce the braced term in Eq. (16) and make it comparable with stabilizing terms that were deleted in deriving the limiting case. Based on the form of the braced term and considering its maximum over all p and q, it was heuristically postulated that a nearly optimal σ_ω should be a function of Re $h^2(\omega_{\max} - \omega_{\min})$, where $\omega_{\max}$ and $\omega_{\min}$ are extreme values of ω over the five-point "cell" involved in the second-order-correct differencing of Eqs. (1) and (2). Further quantification of σ_ω was effected empirically; typical results are discussed below.

Results and Discussion

Convergence/Accuracy Considerations

An objective of the present study was to develop improved computational methods for solving the equations of motion for 2-D recirculating flows at large Reynolds numbers. Owing to onerous coding requirements and/or excessive core-storage demands associated with many existing schemes, the scope of the study was limited to possibilities which emulate, for example, the basic simplicity of the method of false transients, employing simple difference analogs of the governing equations and relaxing the resulting nonlinear algebraic problem by means of, say, ADI methods. Additionally, the trade-offs between computational efficiency and solution accuracy were to be established.

In testing the computational efficiency of the overall method of solution, reliable criteria were needed to monitor errors along the iterative path owing to incomplete convergence of the dependent variables. For hydrodynamic problems of the type considered here, it is our experience that the most appropriate criteria are the so-called "root-mean-square residuals" (RMSR):

$$\mathrm{RMSR}_{\psi} = \left(\sum_{i,j} (\omega + \nabla^2\psi)_{ij}^2/(N-2)^2\right)^{1/2},$$

$$\mathrm{RMSR}_{\omega} = \left(\sum_{i,j} (\mathrm{Re}^{-1}\,\nabla^2\omega - \nabla\cdot\mathbf{v}\omega)_{ij}^2/(N-2)^2\right)^{1/2}.$$

Utilization of these criteria in assessing the effects of variations on the basic method of solution is illustrated in Figs. 2–4.

The effects of uniform vs. non-uniform σ_ω on the approach to convergence of ψ at the cavity center are displayed in Fig. 2, where the error of convergence is here defined as the relative difference between ψ_k, the value existing after the kth iterate, and ψ_∞, the value attained upon achievement of "steady state" (corresponding to the reasonable disappearance of all residuals). The given values of σ_ω and σ_ψ were established empirically to yield near-optimal convergence rates. (Typically, convergence to "steady-state" occurred more slowly for nodes within the main vortex; in general, reduction of these convergence errors to $<1\,\%$ required that the RMSR's be reduced to between 10^{-2} and 10^{-3}. In practice, RMSR's of less than 10^{-4} were attained before convergence was assumed.) Clearly, introduction of nonuniform σ_ω's can effect marked improvements in computational efficiency, particularly as the RMSR's $\to$ 0. Unfortunately, the advantage diminishes rapidly with increasing N, since $h^2(\omega_{\max} - \omega_{\min}) \to 0$ for all nodes points and the σ_ω's approach a (near-optimal) uniform values ($\sim$2); for $N > 81$, very little improvement was observed. Nonetheless, the results were useful in guiding the development of the method of false transients in the (ξ, η) plane. Referring to Eq. (6), it is seen that with

$$\frac{h^2}{\Delta t'_\omega} = \frac{h^2}{\xi_x\eta_y\,\Delta t_\omega} = \sigma_\omega = \text{const},$$

i.e.,

$$\frac{h^2}{\Delta t_\omega} = \sigma_\omega \cdot \xi_x \eta_y$$

there effectively are introduced relatively larger values of the ADI iteration parameter in the near-well regions, since $\xi_x \eta_y$ is a maximum in these regions.

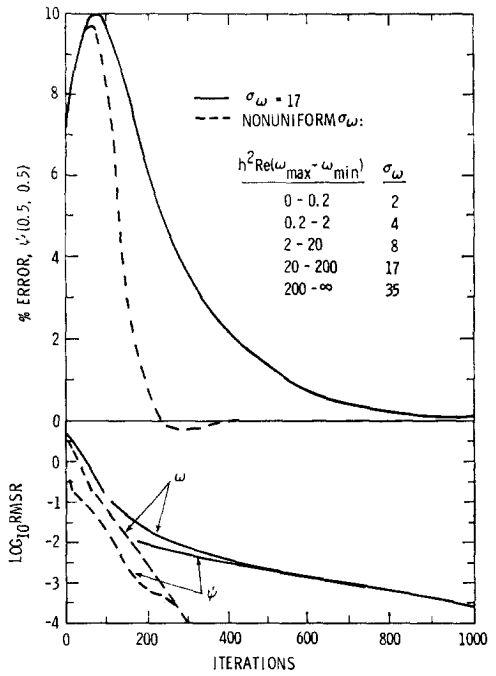

FIG. 2. Effects of uniform versus nonuniform σ_ω on convergence rate: Re = 1600 → 3200, $N = 41$, $\beta = 0$, $\sigma_\psi = 1$, second-order-correct ω_B.

Comparisons of the convergence behavior on solving the problem in (x, y) vs (ξ, η) coordinates, with values of N being selected such that the truncation errors for ψ_{ij} and ω_{ij} are comparable, are displayed in Fig. 3. (Here truncation errors refer to the difference between the completely converged solution for a finite value of N and the "exact" solution corresponding to $N \to \infty$, which is approximated by extrapolation procedures to be described later.) As would be expected, owing to the 2.5-fold reduction in N, convergence is much more efficient for the (ξ, η) formulation.

The behavior of the convergence problem for (ξ, η) coordinates and nonuniform σ_ω at Re = 10^4 is illustrated in Fig. 4 when the RMSR's → 0. Whereas the RMSR's → 0 monotonically, the errors in ψ_{ij} and ω_{ij} decrease via damped oscillations. (Paren-

thetically, it is relevant to note the nearly in-phase extrema in the convergence errors, in Fig. 4, which point up the risk involved in terminating a computation when the solution variables differ negligibly from one iterate to the next.) The behavior in Fig. 4 was typically encountered, in that "timewise" variations effectively disappeared as the RMSR's tended toward zero.

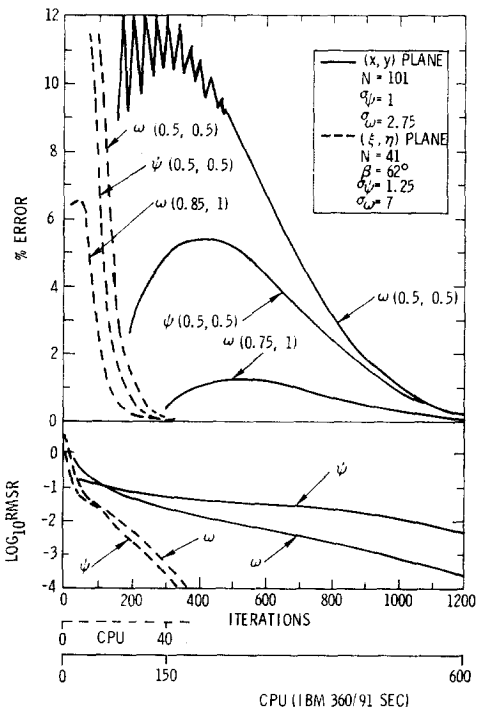

FIG. 3. Comparisons of computational efficiency using (x, y) versus (ξ, η) formulations: errors owing to truncation $\simeq 4\%$. Re = 3200.

In addition to convergence problems at large Re, it is well known [19] that central-difference analogs of the 2-D N–S equations can be subject to spurious spatial oscillations associated with cell Reynolds numbers, Re $h \mid u \mid$ and Re $h \mid v \mid$. As shown in Fig. 5, oscillations of this type did tend to occur for the Re $= 10^4$ case, but these anomolies were removed by suitable choices of N and β.

Another consideration in evaluating the credibility of finite-difference approaches for solving the N–S equations is the extent to which various conserved properties of the flow (vorticity, kinetic energy, square vorticity) are satisfied globally. In the present context, it may be shown [17] that conservation of these properties leads to the following integral constraints.

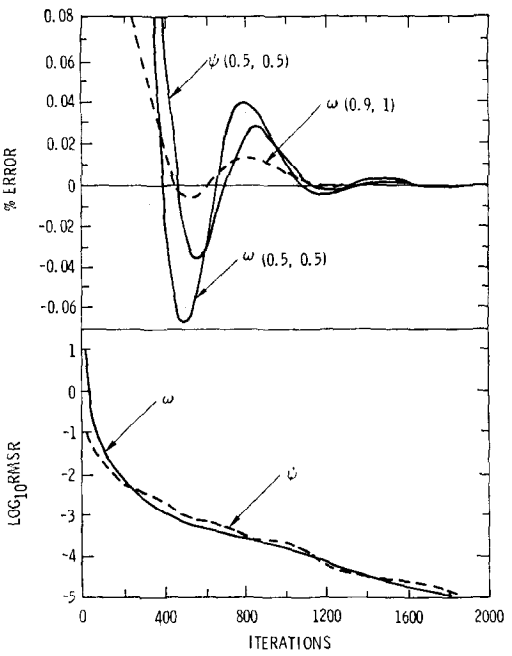

FIG. 4. Convergence behavior as RMSR's $\to 0$: Re $= 10^4$, $N = 81$, $\beta = 72°$, $\sigma_\psi = 4$, $\sigma_\omega = 4, 8, 17$.

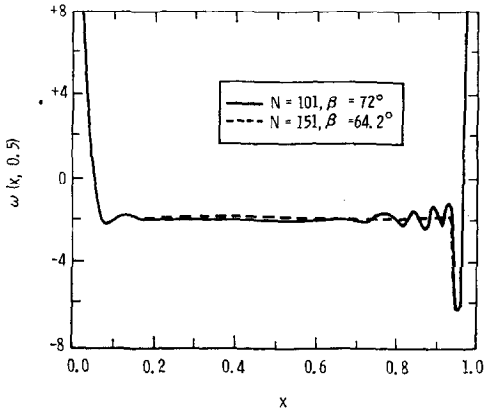

FIG. 5. Effect of parameter choice on spatial integrity, Re $= 10^4$.

Vorticity:

$$\oint_l \nabla\omega \cdot \mathbf{n}\, dl = 0; \tag{17}$$

kinetic energy:

$$\iint_s \omega^2\, ds + \oint_l \omega\, \nabla\psi \cdot \mathbf{n}\, dl = 0; \tag{18}$$

square vorticity:

$$\iint_s \nabla\omega \cdot \nabla\omega \, ds - \oint_l \omega \, \nabla\omega \cdot \mathbf{n} \, dl = 0. \tag{19}$$

The extent to which these integral constraints are satisfied for three well-known alternative formulations of the advective terms in the ω equation

$$(\psi_y\omega)_x - (\psi_x\omega)_y \qquad \text{(divergence)},$$
$$\psi_y\omega_x - \psi_x\omega_y \qquad \text{(convective)},$$
$$\{[(\psi_y\omega)_x - (\psi_x\omega)_y] + [\psi_y\omega_x - \psi_x\omega_y] + [(\psi\omega_x)_y - (\psi\omega_y)_x]\}/3$$

has been explored by solving the governing equations by means of the methods treated here. (Application of three-point central-difference approximations to the third expression results in Arakawa's conservative scheme for the advective terms.) Evaluation of Eqs. (17)–(19) was effected by means of trapezoidal quadrature, employing discrete data from the converged numerical solutions. From an overall standpoint, the divergence formulation resulted in minimal errors in enforcing global conservation of the given properties, the Arakawa "conservative" scheme proving to be less satisfactory owing to problems in enforcing conservation at solid boundaries. As expected, the convective scheme proved least satisfactory as a result of rather large errors in conserving square vorticity. Further details appear in [17].

Of further interest is the effect of the order correctness of the vorticity boundary condition on the accuracy of the numerical solution. For $N = 41$ and $\beta = 0$, with $\mathrm{Re} = 1000$, the percent errors in $\psi(0.5, 0.5)$ owing to truncation were -10.3, 7.0, and 6.4 on using first-, second-, and third-order-correct boundary conditions, respectively; while, those for $\omega(0.5, 0.5)$ were -9.3, -6.8, and -6.6. With increasing N, the error spread is, expectedly, reduced.

Converged Solutions of the Governing Equations

Numerical solutions of the governing equations were obtained at Reynolds numbers ranging from 10^3 to 10^4. The basic data, consisting of 2-D arrays for ψ_{ij} to six significant figures, has been preserved on cards for the "best" solution at each Re.

The effects of increased Re on the basic structure of the recirculating flow are illustrated in Figs. 6 and 7, with numerical values of the more significant flow properties being given in Table I. The "exact" values at $h \to 0$ were obtained by means of h^n extrapolation, wherein solutions at three different mesh spacings, h, were used to establish the intercept, a, of a flow variable, ϕ, in the equation $\phi = a + b \cdot h^n$. Typically, values of n varied between 1.50 and 1.75 (see Fig. 8), illustrating the influence of the singularities in the upper corners in reducing the effective order correctness of the solution procedure.

Of particular interest is that the best obtained solutions for ψ and ω in the center of the main vortex and ω on the top plate at $\mathrm{Re} = 3200$ and 10,000 are all within 1 %

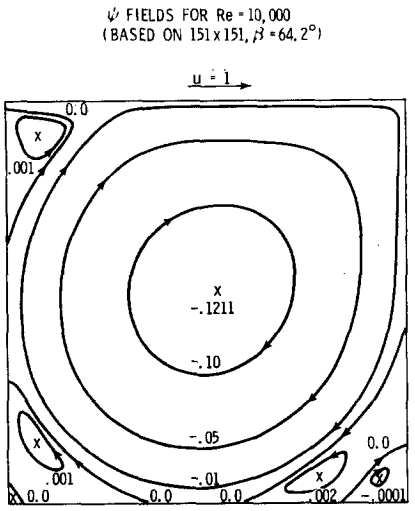

FIG. 6. Flow structure at Re = 10^4: $N = 151$, $\beta = 64.2°$.

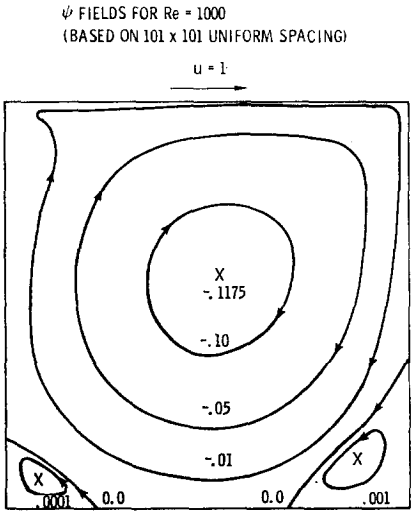

FIG. 7. Flow structure at Re = 10^3: $N = 101$, $\beta = 0$.

of the corresponding values for $h = 0$ obtained by extrapolation, this high degree of accuracy being directly attributable to the resolution of the boundary layer regions afforded through the coordinate transformation. Also of interest are the trends in ψ and ω at the center of the main vortex, where ψ apparently has attained an asymptotic value (-0.212) and ω is approaching the asymptotic value -1.86, as estimated by extrapolating the Re = 10^3, 3.2×10^3, 10^4 results to very large Reynolds numbers.

TABLE I

Derived Properties of Converged Solutions

Re	1000		3200		10000	
N (node points) β (degrees)	101 0	Extrapolated[a] 0	101 65.2	Extrapolated[a] 0	151 64.2	Extrapolated[b] 72
ψ values at vortex centers						
Primary vortex	−0.1175	−0.1193	−0.1210	−0.1217	−0.1211	−0.1212
Secondary vortex (lower right)	0.001752	0.001724	0.002879	0.002807	0.003270	0.002948
Secondary vortex (lower left)	0.000229	0.000233	0.001114	0.001083	0.001606	0.001597
Secondary vortex (upper left)	None		0.000704	0.000723	0.002585	0.002711
Tertiary vortex (lower right)	-2×10^{-8}		-2×10^{-7}		−0.000124	−0.000110
Tertiary vortex (lower left)	None		-4×10^{-8}		-9×10^{-7}	-9×10^{-7}
Fourth-order vortex (lower right)	None		None		3×10^{-9}	
Core vorticity	−2.044	−2.078	−1.949	−1.957	−1.900	−1.885
Minimum vorticity (top plate)	−14.13	−14.07	−24.58	−24.23	−43.94	−43.45
CPU seconds (IBM 360/91)	260		1110		5280	

[a] From solutions at $N = 61, 81, 101$.
[b] From solutions at $N = 71, 81, 101$.

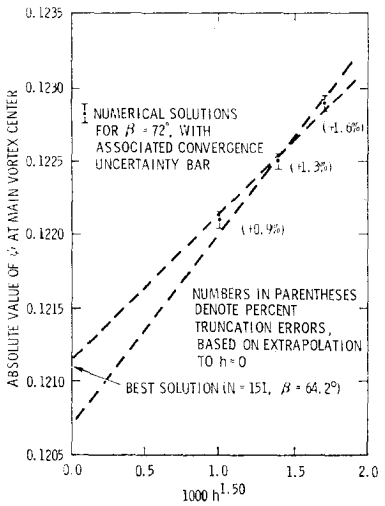

FIG. 8. Illustration of truncation error determination for Re $= 10^4$.

The latter result is very close to the analytical value (-1.886) calculated by Burggraf [2] in his application of Batchelor's model [20], consisting of an inviscid core with uniform vorticity, coupled to boundary layer flows at the solid surfaces. As expected, the present results at large Re indeed establish a large central region of essentially constant vorticity; however, the existence of secondary vortices of modest strengths in the corners would, expectedly, yield a slightly different value of the asymptote for $|\omega|$ as Re $\to \infty$. Other parameters of interest, such as centerline velocity distribution and vortex center location versus Re, are similar to previous results [2, 3, 8] and, therefore, are not shown here.

Owing to mesh-size limitations, quantitative assessment of the detailed properties of the secondary vortices with increasing Re is slightly less satisfactory. Nonetheless, it is clear that the ψ values are approaching asymptotes; e.g., the value of $\psi_{\max}$ within the well-developed lower-right vortex at Re $= 10^4$ (2.95×10^{-3}) is near the estimated value at Re $\to \infty$ (3×10^{-3}). Furthermore, we confirm an earlier inference by Mallinson and deVahl Davis [16] wherein the secondary vortex in the upper left corner is generated at a critical Reynolds number, estimated here to be $\sim$1200.

The persistence and, indeed, enlargement of the secondary vortices with increasing Reynolds number up to Re $= 10^4$ is a feature of the present solutions that differs from other published results [3, 8], which were obtained by using a lower-order correct upwind difference scheme in connection with the convective form of the vorticity equation. As shown in Fig. 9, results obtained with the upwind-differenced-convective (UDC) scheme would lead to the conclusion that the secondary vortices begin to diminish at high enough Reynolds numbers and eventually disappear, whereas the present results, using a centrally-differenced-divergence (CDD) method, show no

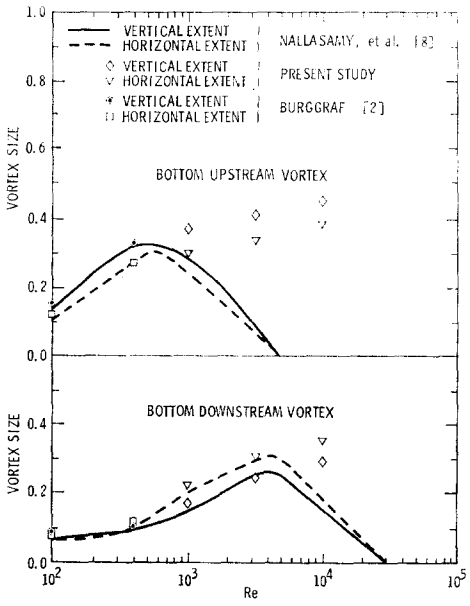

FIG. 9. Comparisons of secondary vortex sizes as a function of Reynolds number.

such inclination. The conflict occurs only for Re $>$ 500 for the bottom upstream vortex and Re $>$ 4000 for the bottom downstream vortex, which explains why Burggraf's numerical results for Re $\leqslant$ 400 are in agreement with both methods (see Fig. 9).

Contrary to the idea that the secondary vortices disappear at high enough Re, the present results suggest that as Re $\rightarrow \infty$, the primary vortex becomes a centrally located increasingly circular region of constant vorticity, essentially circumscribed by the boundaries of the cavity. A series of counterrotating vortices occupies each of the lower corners, with the vertical and horizontal extents of the largest of these apparently approaching 0.5. (This picture of the flow structure in the stationary lower corners is in agreement with Moffatt's analytically derived model of an infinite series of rapidly diminishing counterrotating vortices [21].)

Experimentally, there is little data available for 2-D cavities at high Reynolds numbers; and that which is available has been questioned [4, 10]. The experiments of Pan and Acrivos [22] indicate a secondary vortex in the lower right (upstream) corner which decreases in size as Re increases beyond 500, in apparent disagreement with the present results. However, their experiments also imply that no secondary vortex exists in the lower left (downstream) corner up to Re = 2700 (their maximum value), which contradicts both the present results and all the previously referenced numerical studies. A possible explanation for this behavior, offered in [4, 10], is that the experimental apparatus was such as to introduce vertical components of velocity at the upper boundary, owing to the use of a circular drum to form the sliding upper

surface. Since the drum protruded into the cavity to about 17 % of the cavity depth, it was postulated that induced vertical velocities could have had an effect on the secondary vortices. It is pertinent that the earlier experiments of Mills [23], using a flat belt arrangement for the upper surface, indicated secondary vortices remaining in both the upstream and downstream lower corners at $\mathrm{Re} = 10^5$. According to [4], however, both sets of experiments were likely subject to significant three-dimensional effects, making them inappropriate as standards for comparison with numerical solutions of the two-dimensional problem.

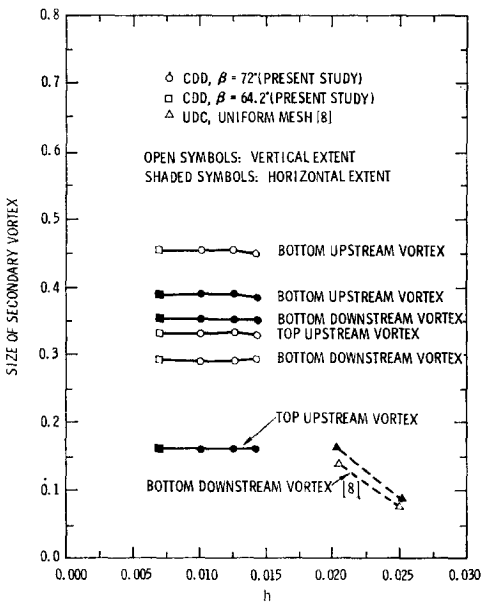

FIG. 10. Comparisons of mesh size effect on secondary vortex size. $\mathrm{Re} = 10^4$.

In view of the differences in the results for CDD and UDC, as well as the available experimental data, it becomes important to examine the truncation errors in the regions of the secondary vortices to determine the extent to which these solutions depart from the "steady-state" solution of the differential equations, (1) and (2). Figure 10 shows that the sizes of all of the secondary vortices obtained by CDD in the present study have definitely attained limiting values (i.e., further reductions in h would provide no significant improvements); whereas, the bottom downstream vortex size obtained by UDC and reported in [8] is still highly influenced by node spacing for the ranges of h considered there. If much smaller mesh sizes were used in [8], one could surmise from Fig. 10 that the size of the vortex would become significantly larger.

To explore the behavior of the truncation errors in both methods of solution, it

may be shown that the lowest-order errors for UDC evolve from the advective terms, are proportional to h, and are given by

$$E_{\mathrm{UDC}} = \frac{h}{2}\left(\left|\frac{\partial\psi}{\partial y}\right|\frac{\partial^2\omega}{\partial x^2} + \left|\frac{\partial\psi}{\partial x}\right|\frac{\partial^2\omega}{\partial y^2}\right) + O(h^2), \tag{20}$$

whereas those for CDD (also evolving from the advective terms) are proportional to h^2 and are given by

$$E_{\mathrm{CDD}} = \frac{h^2}{6}\left[\frac{\partial^3}{\partial\xi^3}\left(\frac{\partial\psi}{\partial\eta}\,\omega\right) - \frac{\partial}{\partial\eta}\left(\frac{\partial^3\psi}{\partial\xi^3}\,\omega\right) - \frac{\partial^3}{\partial\eta^3}\left(\frac{\partial\psi}{\partial\xi}\,\omega\right) + \frac{\partial}{\partial\xi}\left(\frac{\partial^3\psi}{\partial\eta^3}\,\omega\right)\right]\frac{d\xi}{dx}\frac{d\eta}{dy} + O(h^4), \tag{21}$$

where Eq. (21) includes the coordinate transformation to (ξ, η). Using the best available finite-difference solution (CDD, $N = 151$, $\beta = 64.2°$) to numerically determine appropriate derivatives at $\mathrm{Re} = 10^4$, a comparison of E_{UDC} and E_{CDD} with the diffusion term $\mathrm{Re}^{-1}\nabla^2\omega$ was made along the vertical line $x = 0.075$. (This line was chosen because of its nearness to the centers of the two left-side secondary vortices.) As shown in Fig. 11, the truncation errors accruing with the UDC method used in [8]

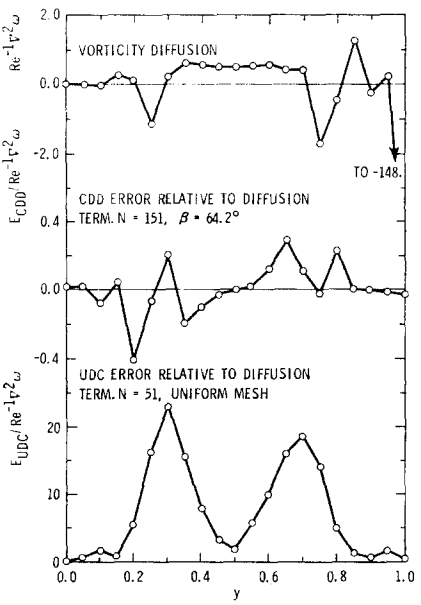

FIG. 11. Comparisons of CDD and UDC lowest-order advection truncation errors with vorticity diffusion term. $\mathrm{Re} = 10^4$, $x = 0.075$.

are as much as 25 times greater than the magnitude of the diffusion term and are always in the same direction; thus, they effectively decrease (in a nonuniform way) the apparent Reynolds number. On the other hand, the CDD errors in the present contribution do not exceed 0.4 times the diffusion term, and they occur equally in both directions relative to the diffusion term. Thus the differences in the secondary vortex patterns occurring in [8], as compared to the present study, are due to the fact that the truncation errors in [8] are approximately 60 times as great as those in the present study. (Parenthetically, if $N = 151$ had been used with UDC, the errors would still be as much as eight times the diffusion term, since E_{UDC} is proportional to h.)

As a final note, the use of laminar flow equations up to $\text{Re} = 10^4$ is predicated on the fact that there is no conclusive experimental evidence available for recirculating flow in a 2-D square cavity to indicate that a transition to turbulence occurs at a lower Reynolds number. Clearly, it would be desirable for both experiments and flow stability analyses to be conducted to determine the critical Reynolds number for this geometry and flow situation. In any flow stability analysis, reliable solutions of the laminar flow equations will be required.

REFERENCES

1. R. D. MILLS, *J. Roy. Aeron. Soc. London* **69** (1965), 714–718.
2. O. R. BURGGRAF, *J. Fluid Mech.* **24** (1966), 113–151.
3. J. D. BOZEMAN AND C. DALTON, *J. Computational Phys.* **12** (1973), 348–363.
4. G. DE VAHL DAVIS AND G. D. MALLINSON, *Computers and Fluids*, **4** (1976), 29–43.
5. K. N. GHIA, W. L. HANKEY, AND J. K. HODGE, Study of incompressible Navier–Stokes equations in primitive variables using implicit numerical technique, presented at AIAA 3rd Computational Fluid Dynamics Meeting, 1977.
6. D. GREENSPAN, *Computer J.* **12** (1969), 89–94.
7. A. D. GOSMAN, W. M. PUN, A. K. RUNCHAL, D. B. SPALDING, AND M. WOLFSHTEIN, "Heat and Mass Transfer in Recirculating Flows," Academic Press, London/New York, 1969.
8. M. NALLASAMY AND K. KRISHNA PRASAD, *J. Fluid Mech.* **79** (1977), 391–414.
9. H. Z. BARAKAT AND J. A. CLARK, Analytical and experimental study of transient laminar natural convection flows in partially filled containers, in Proc. 3rd Int. Heat Transfer Conf., Vol. II, pp. 152–162, 1966.
10. S. Y. TUANN AND M. D. OLSON, *J. Computational Phys.* **29** (1978), 1–19.
11. J. E. FROMM, *IBM J. Res. Develop.* **7** (1971), 32–45.
12. D. W. PEACEMAN AND H. H. RACHFORD, JR., *J. Soc. Indust. Appl. Math.* **3** (1955), 28–41.
13. A. J. CHORIN, *J. Fluid Mech.* **57** (1973), 785–796.
14. A. I. SHESTAKOV, A hybrid vortex–ADI solution for flows of low viscosity, Lawrence Livermore Laboratory Report, UCRL 81036, 1978.
15. V. E. DENNY AND R. M. CLEVER, *J. Computational Phys.* **16** (1974), 271–284.
16. G. D. MALLINSON AND G. DE VAHL DAVIS, *J. Computational Phys.* **12** (1973), 435–461.
17. A. S. BENJAMIN, Finite difference solution of recirculating flow in a two-dimensional cavity at high Reynolds number, Ph.D. thesis, UCLA, 1977.
18. R. W. JOHNSON AND A. M. DHANAK, A.S.M.E. Paper 75-HT-58, AIChE/ASME Heat Transfer Conference, San Francisco, August 11–13, 1975.

19. P. J. ROACHE, "Computational Fluid Dynamics," Hermosa Publishers, Albuquerque, 1972).
20. G. K. BATCHELOR, *J. Fluid Mech.* **1** (1956), 177–190.
21. H. K. MOFFAT, *J. Fluid Mech.* **18** (1964), 1–18.
22. F. PAN AND A. ACRIVOS, *J. Fluid Mech.* **28** (1967), 643–655.
23. R. D. MILLS, *J. Roy. Aeron. Soc. London* **69** (1965), 116–120.